第51卷第11期 中国科学技术大学学报 Vol. 51, No. 11
2021年11月 JOURNAL OF UNIVERSITY OF SCIENCE AND TECHNOLOGY OF CHINA Nov. 2021
Received: 2021-09-06; Revised: 2021-09-23 doi:10.52396/JUST-2021-0195

Sequence-dependent hybridizability of DNA-monoconjugated nanoparticles: Kinetic complexity unveiled by a dimerization assay

WANG Jiannan, ZHENG Yuanqin, LI Yulin, DENG Zhaoxiang*
Center for Bioanalytical Chemistry, Department of Chemistry, University of Science and Technology of China, Hefei 230026, China
* Corresponding author. E-mail: zhxdeng@ustc.edu.cn

Abstract: Understanding DNA hybridization kinetics is highly important for nucleic acid detections, genomic biotechniques, and DNA nanotechnology. DNA-conjugated nanomaterials offer versatile functionalities for DNA-programmable nanoassembly with superfine controls toward bioanalytical and nanotechnological applications. Although small molecule end-tagging does not incur much attenuation of DNA's hybridizability, nanoparticle-conjugation greatly suppresses the hybridization kinetics of DNA strands. The impeded hybridization not only decreases the efficiency in building complicated nanostructures, but also causes difficulty in realizing rapidly responsive sensors and nanomotors. With monovalent DNA-nanoparticle conjugates as an ideal system, this work aims to unveil the kinetic complexity of hybridization-driven dimeric assembly assayed by agarose gel electrophoresis. Our results point out a coexistence of different factors that can affect the hybridization kinetics of DNA-conjugated nanoparticles, including: the rigidity of a DNA spacer proximal to the nanoparticle surface; the base-stacking between the spacer and a hybridized domain; the inherent base-sequence-dependent DNA hybridizability; and the spatially confined movement of the hybridization sequences. The dimeric hybridization assay offers a reliable platform for kinetic evaluation of DNA-conjugated nanoparticles to enable structurally complicated and rapidly functioning analytical devices and bio-labelling nanoprobes.
Keywords: electrophoresis; DNA; hybridization kinetics; nanoparticles; monoconjugates
CLC number: Q523; TB383.1 **Document code**: A

1 Introduction

DNA nanotechnology is a rapidly evolving scientific field aiming at providing a highly programmable self-assembly strategy for the bottom-up nanostructural control based on DNA supramolecular chemistry[1-3]. One major goal in this area is to build static as well as dynamic nanostructures with prescribed functions toward metamaterials[4-6], chemo/biosensors[7-9], and nanomotors[10,11]. Due to a lack of explicit functions of DNA molecules in the contexts of chemistry and materials science, great efforts have been invested in the development of DNA-conjugated nanomaterials[12-23]. One research focus is centered on the valency control of DNA-nanoparticle (NP) conjugates, which determines nanoparticles' ability to form topologically well-defined nanomolecules[24]. Apart from multivalent DNA-NP complexes[25], DNA-monofunctionalized materials are especially important[14-19,23,24]. The monovalent DNA-NP conjugate is more like a "hydrogen atom" that exists in almost every "nanomolecule". With DNA nanostructures as scaffolds, virtually any structural geometries free from crosslinking errors can be created for nanoparticle assemblies based on DNA-NP monoconjugates. In addition, the monovalent DNA-nanoparticle complexes strictly allow a 1 : 1 target recognition, offering excellent nanoprobes for chemical/biological sensing and single-molecule tracking without causing erroneous dynamic information or triggering cellular lysis due to multivalent binding[26] and crosslinking[27].

A good hybridizability of DNA is desired for DNA-programmable, functioning nanodevices[28-38]. Understanding DNA hybridization kinetics is also highly important for gene-related biotechniques and nucleic acid detections[39-48]. The facilitated hybridization not only contributes to fast-responding sensors but also allows the building of complicated and kinetically unfavorable nanostructures. Mirkin et al. suggested a freezing-thawing strategy to achieve a rapid aggregation of DNA-functionalized AuNPs for a colorimetric sensing of DNA[31]. Hamad-Schifferli et al. used

Citation: Wang Jiannan, Zheng Yuanqin, Li Yulin, et al. Sequence-dependent hybridizability of DNA-monoconjugated nanoparticles: Kinetic complexity unveiled by a dimerization assay. J. Univ. Sci. Tech. China, 2021, 51(11): 802-812.

mercaptohexanol (MCH) backfilling on DNA-multifunctionalized AuNPs to improve their hybridizations by suppressing adsorptive DNA conformation[32]. This idea was recently revisited by Liu et al. who found that bromide ion was a much better backfiller than MCH in improving DNA's hybridizations on AuNPs[33]. Gang et al. employed a DNA duplex spacer to extend a DNA hybridization domain farther away from AuNP surface such that reduced chain entropy and base adsorption and therefore an almost doubled hybridization speed were achieved[34]. Mirkin et al. found that a short complement DNA hybridized to one part of a DNA sequence close to nanoparticle surface could significantly improve DNA hybridization via a strand-displacement reaction[35]. We previously reported the use of a triblock DNA ligand featuring a duplex domain flanked by anchoring and hybridizing DNA tracts to achieve largely improved DNA hybridization on single walled carbon nanotubes (SWNTs)[36]. The improved hybridization kinetics was found critically important for DNA-guided alignment of SWNTs into functioning devices[37,38].

Despite the inspiring results achieved before, most of them are limited to DNA-multifunctionalized NPs. As a result, the kinetic hindrance of DNA hybridization is mainly attributed to the crowding, surface adsorption, and self-folding of DNA ligands grafted on NPs[28-48], which overwhelm the inherent kinetic complexity related to base sequences. We attribute this limitation to the unavailability of ideal DNA-NP conjugates and a technical difficulty in accurately quantifying their hybridization kinetics based on a reliable kinetic model. In the case of monovalent DNA-NP conjugates, the DNA grafting density would no longer be an issue affecting their hybridizations, which, however, plays a crucial role for multifunctionalized DNA-NP conjugates. Therefore, experimentally observed kinetic consequences can be narrowed down to disclose the often overlooked sequence-dependency of DNA's hybridizability on NPs. In addition, DNA density measurement on NPs is sometimes a tricky job with significant quantitation errors, which is not a problem for monovalent DNA-NP complexes. In fact, the as-measured DNA density is a statistical average hard to reproduce in a different experiment. Also, the DNA loading always fluctuates on different NPs in the same solution. Especially, the hybridized products (NP aggregates) of multifunctional DNA-NP conjugates have a wide size distribution and largely varied morphologies, raising a big challenge in finding a suitable kinetic model. In contrast, monovalent DNA-NP conjugates are well-suited for kinetic comparisons among different systems benefiting from their structural simplicity, reproducibility, and uniformity. As a result, kinetic effects due to a minor sequence change may be easily discriminated. Along this line, the increased availability of DNA-NP monoconjugates and their applicability in biosensing and nanotechnology call for a strict kinetic evaluation of the emerging class of valence-controllable bio-nano-conjugates[14-19,23,24,49].

With improved NP syntheses and DNA conjugation, we can reduce the minimal DNA length to about 30 bases which still allow a gel electrophoretic DNA-valence separation (Figure S1). Such a significant improvement surpasses a previously reported record of about 50 bases in the case of 5 nm AuNPs[50,51]. The greatly shortened DNA length would alleviate kinetic complications from self-folded ligand conformations[52-54]. Also thanks to the DNA monovalency, only dimeric products will be formed during DNA-driven nanoassembly[24,55]. Therefore, a simple homogeneous second-order chemical kinetics can be borrowed to model the hybridization-driven NP assembly. Note again previous studies with multifunctional DNA-AuNP "reactants" produced infinite numbers of NP aggregates ("products") with different sizes and 3D conformations, making it hard to formulate the self-assembly kinetics. While an aggregation-based system could take advantage of plasmonic color transitions of AuNPs to monitor DNA hybridization[31,34], we can employ a more quantitative and reliable agarose gel electrophoretic (AGE) assay to determine the dimerization rates. As well, our process does not need any fluorescent labels which might affect the DNA hybridization and easily get photo-bleached during an optical measurement.

2 Materials and methods

Five pairs of complementary DNA strands (referred to as systems 1 to 5) were chosen for the kinetic measurements. The complementarity between the DNA strands was verified by non-denaturing polyacrylamide gel electrophoresis (PAGE) (Figures S2-S6). Two basic rules were strictly followed during the sequence design: (i) a relatively short (15 bases) hybridization segment as a terminal part of the DNA ligand, plus a 15-base long ploy-T spacer (T_{15}) as a proximal domain to the gold surface; (ii) minimized DNA self-folding to avoid secondary conformations which are well-known kinetic barriers for DNA hybridization. The purpose of the rules was to exclude potentially unknown factors that might affect DNA hybridization in order to zero in on the kinetic effects of spacer rigidity (single and double stranded), base stacking, and base sequence. Spacer

rigidity determines the distance of a hybridization event away from the NP surface. The role of base-stacking is often manifested when a "nicked" DNA duplex can still maintain a good stability against dissociation. However, the sequence effect (not related to any secondary conformations) has not been well studied on nanoparticles so far (but very important in practice). Our experiments began with an incubation of thiolated DNA strands with 5 nm AuNPs capped by Bis (*p*-sulfonatophenyl) phenylphosphine (BSPP), followed by a gel electrophoretic isolation of DNA-monoconjugated AuNPs. Two parts of the gel-purified DNA-AuNP complements were combined to initiate dimeric NP assembly. The product yields at different reaction stages were quantified by an AGE assay. The correct formation of the AuNP dimers was verified by transmission electron microscopy imaging (Figures S7−S11).

Benefiting from the simplicity of our systems (Scheme 1), the hybridization between two univalent DNA-AuNP conjugates can be modeled as a homogeneous second-order chemical reaction:

$$A + B \xrightarrow{k_{app}} P \qquad (1)$$

where A and B represent AuNP monomers bearing complementary DNA ligands, P is the hybridized dimer product, and k_{app} is an apparent second-order kinetic constant. The initial concentrations of A and B were made equal (i.e. $[A]_0 = [B]_0$) in our experiments. Note that the dissociation reaction is ignored considering the good stability of the dimer products[54]. Actually, the as-formed nanoparticle dimers did not undergo an observable disassembly during gel electrophoreses and TEM sample preparations due to their high melting points (ca. 40 − 50 ℃) relative to hybridization temperatures (room temperature and 4 ℃). Based on this assumption, the following formula can be derived to account for the product concentration as a function of the reaction time:

$$\frac{[A]_0}{[P]} = \frac{1}{k_{app}[A]_0} \cdot \frac{1}{t} + 1 \qquad (2)$$

Since $[A]_0/[P]$ is a reciprocal of the reaction yield Y, Eq. (2) can be rewritten as:

$$\frac{1}{Y} = \frac{1}{k_{app}[A]_0} \cdot \frac{1}{t} + 1 \qquad (3)$$

By plotting $1/Y$ versus $1/t$, k_{app} can be obtained from the slope of a linear fitting of experimental data.

3 Results and discussion

We first employed the DNA sequences (termed as system 1) originally adopted by Gang et al. to study

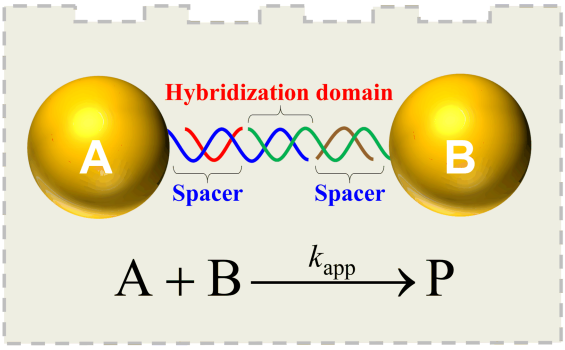

Scheme 1. Agarose gel electrophoresis (AGE) based hybridization assay reveals a sequence-dependent kinetic complexity of DNA-monoconjugated gold nanoparticles.

DNA hybridization kinetics[34]. This system previously exhibited a 2-fold kinetic enhancement upon introducing a polyA (A_{15}) DNA to pair with the T_{15} spacer. By choosing system 1, we were curious to see if the above fact would still hold for DNA-monoconjugated AuNPs during a dimeric assembly (instead of random NP aggregation). As shown in Figure 1 (a), the dimerization was significantly accelerated for the DNA-AuNP monoconjugates with double-stranded spacers in proximity to AuNP surface. The kinetic improvement was more conveniently judged from Figure 1(b), where the logarithmic intensities of gel bands were converted into optical densities. To obtain the peak areas for the dimers and monomers based on the digitalized electropherograms, a Gaussian fitting was conducted to deconvolute slightly overlapped reactant and product bands. The dimerization yield (Y) was then obtained based on the following relationship:

$$Y = \frac{A_{dimer}}{A_{dimer} + A_{monomer}} \qquad (4)$$

where A_{dimer} and $A_{monomer}$ represent the peak areas of the dimers and monomers, respectively. Therefore, Eq. (3) could be plotted with $1/Y$ as a linear function of $1/t$, which was shown in Figure 1(b). The 1 min data were not accurate due to a difficulty to catch such a quick process, which were not included in the data plots. Linear least square (LLS) fitting of the kinetic data gave k_{app} constants for system 1 based on Eq. (3). At room temperature (18 ℃), the DNA ligands with single stranded polyT spacers had a second-order reaction constant $k_{app}^{ss} = 7.55\times10^7$ L · mol^{-1} · h^{-1}, in contrast to the same DNA strands with duplex spacers which resulted in a k_{app}^{ds} of 1.67×10^8 L · mol^{-1} · h^{-1}. Therefore, the use of a rigid duplex spacer led to doubled hybridizability for the DNA-NP conjugates of system 1. Interestingly, when the hybridization was carried at a lowered temperature of 4 ℃, such a kinetic

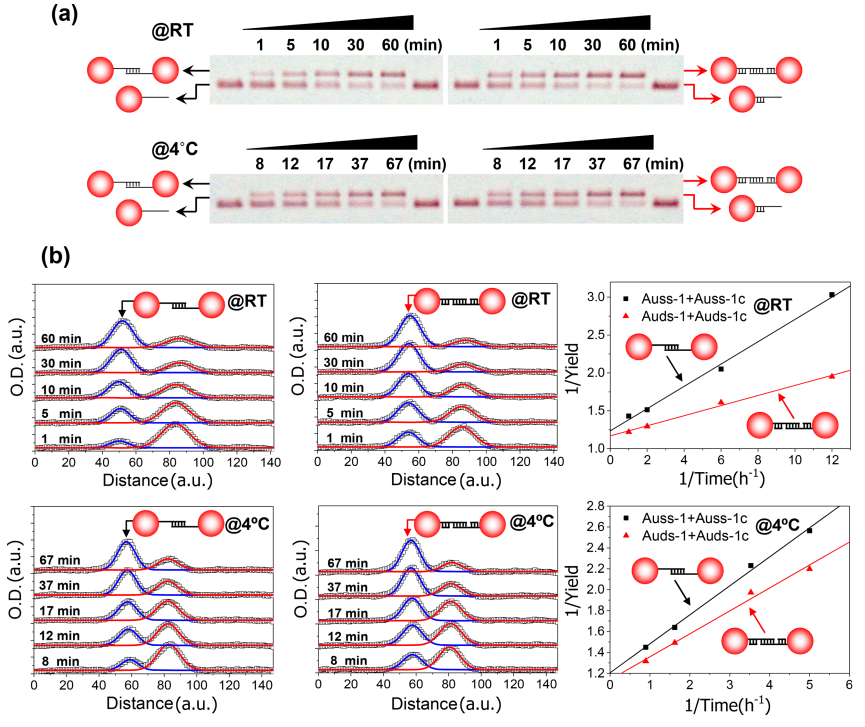

Figure 1. Gel electrophoretic analysis of the hybridization kinetics for system 1. (a) 3% agarose gel electrophoretic separations of the dimerization products of 5 nm gold nanoparticles corresponding to different reaction durations. Each nanoparticle bears a single DNA ligand with an either single or double stranded DNA spacer domain proximal to the gold surface. (b) Digitized gel electropherograms and corresponding kinetic plots to extract kinetic constants. DNA sequences for system 1: ss-1: TACTTCCAATCCAAT-T_{15}-SH (5'-3'); ss-1c: ATTGGATTGGAAGTA-T_{15}-SH (5'-3'). The double stranded spacer is formed by hybridizing ss-1 and ss-1c with an A_{15} complement. Auss and Auds represent DNA-monoconjugated AuNPs with single and doubled stranded spacer domains, respectively.

difference became quite marginal (k_{app}^{ss} = 4.01×10^7 L·mol^{-1}·h^{-1} and k_{app}^{ds} = 5.06×10^7 L·mol^{-1}·h^{-1}).

The consistency of our results with the previous study by Gang et al. evidenced the reliability of our experiments[34]. The results from system 1 indicated that the duplex spacer was still effective in improving the hybridizability of DNA-monoconjugated AuNPs, where ligand crowding did not exist due to DNA monovalency. Therefore, the enhanced DNA hybridizability by a duplex spacer might be attributed to the suppressed DNA adsorption (transient or permanent) on the AuNPs. Such an effect could be understood through a geometric model shown in Figure S12. The duplex spacer of the DNA ligand had a length of ca. 5.1 nm (15 bases), close to the size (diameter) of the AuNPs. Such a rigid rod (a duplex has a persistence length of 50 nm) resulted in a steric hindrance which kept the hybridization event away from the AuNP surface to avoid an adsorption. Another important factor should be the base stacking at the interface between the double stranded spacer and hybridization domains (see Scheme 1), which is known to facilitate DNA hybridization[56]. These two scenarios explained the effectiveness of the duplex spacer in promoting the dimerization kinetics.

Our results gave a clear understanding of the adsorptive kinetic barrier during a DNA-mediated dimeric NP assembly based on monovalent DNA-AuNP conjugates (Figure S12), which had not been revealed before. Such a conclusion is reliable due to the simplicity of our system that excludes kinetic contributions from different DNA grafting densities and self-folded DNA conformations. To explore the generality of the duplex spacer strategy and disclose the base-sequence-dependent dimerization kinetics, we altered the base sequences of system 1 while maintaining the same base compositions. The resulting DNA strands were termed as system 2 based on which kinetic data were obtained (Figure 2). This system revealed some important results. First, a simple alteration of the base orders in the hybridization domains greatly slowed down the dimerization reaction. Accordingly, k_{app}^{ss} and k_{app}^{ds} were decreased to 2.62×10^7 and 6.52×10^7 L·mol^{-1}·h^{-1} at room temperature (18 ℃), respectively. This meant a roughly 2 to 3-fold kinetic suppression for system 2. Considering that systems 1 and 2 had identical base compositions, such a phenomenon pointed to a strong sequence-dependency of the DNA adsorption and hybridization events. Second, at a lowered temperature of 4 ℃, the k_{app}^{ss} and k_{app}^{ds} decreased to 1.01×10^7 L·

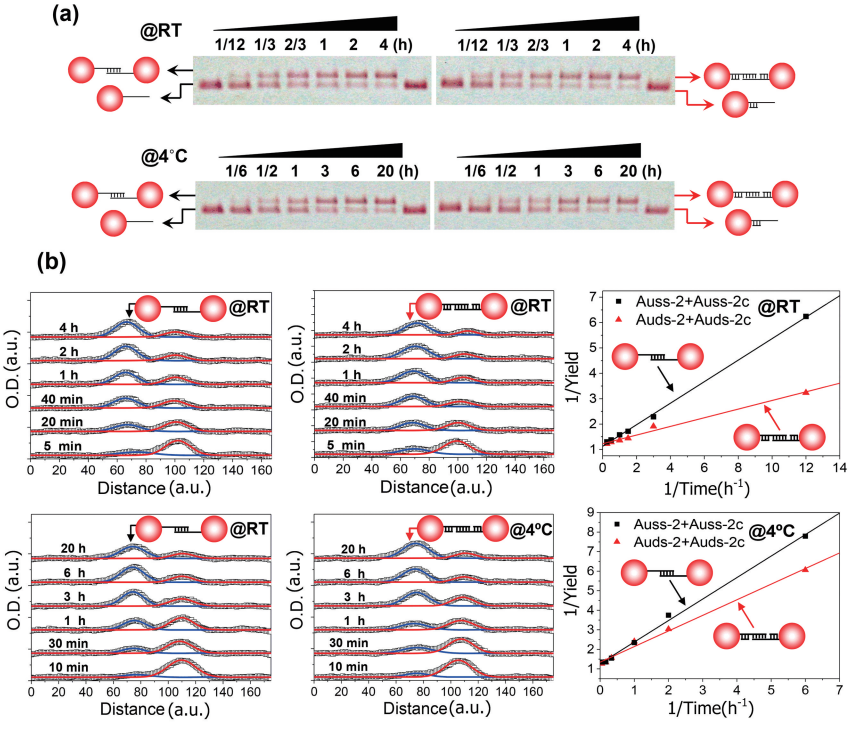

Figure 2. Gel electrophoretic analysis of the hybridization kinetics for system 2. (a) 3% agarose gel electrophoretic separations of the dimerization products of 5 nm gold nanoparticles corresponding to different reaction durations. Each nanoparticle bears a single DNA ligand with an either single or double stranded DNA spacer domain proximal to the gold surface. (b) Digitized gel electropherograms and corresponding kinetic plots to extract kinetic constants. DNA sequences for system 2: ss-2: TCTAACTCCATCATA-T_{15}-SH (5'-3'); ss-2c: TATGATGGAGTTAGA-T_{15}-SH (5'-3'). The double stranded spacer is formed by hybridizing ss-2 and ss-2c with an A_{15} complement. Auss and Auds represent DNA-monoconjugated AuNPs with single and doubled stranded spacer domains, respectively.

$mol^{-1} \cdot h^{-1}$ and 1.39×10^7 $L \cdot mol^{-1} \cdot h^{-1}$, respectively, with a less prominent kinetic difference between the single and double stranded DNA ligands. The negligible kinetic improvement at 4 ℃ for both systems 1 and 2 by the use of a duplex spacer suggested that base stacking (instead of adsorption) probably played a major role in the facilitated kinetics. This implication was reasonable considering that the base stacking effect should be less critical at 4 ℃ where the DNA hybrids do not need its help to get "over-stabilized". Another fact in support of this argument is that DNA adsorption on BSPP-passivated AuNPs is relatively weak due to the stable Au-P bonding. Therefore, the minor adsorption of nucleobases on gold might not be a determining factor in affecting DNA hybridization.

Considering the prominent sequence effect, we purposely modified the base compositions of the terminal hybridization regions to generate systems 3 and 4. We should emphasize again that we tried to avoid a sequence that tends to fold into a stable hairpin or other undesired conformations to avoid the known kinetic complications. Two important clues could be inferred from the kinetic data of these two systems (Figures 3 and 4). In the case of system 3, both k_{app}^{ss} (4.01×10^7 $L \cdot mol^{-1} \cdot h^{-1}$) and k_{app}^{ds} (3.24×10^7 $L \cdot mol^{-1} \cdot h^{-1}$) became smaller compared to the previous systems, with an even negligible difference for single and double stranded spacers. Interestingly, the negligible difference between k_{app}^{ss} and k_{app}^{ds} with a reversed kinetic order at room temperature (18 ℃) was enhanced when the hybridization temperature was lowered to 4 ℃ (k_{app}^{ss} = 3.95×10^6 $L \cdot mol^{-1} \cdot h^{-1}$, k_{app}^{ds} = 1.31×10^6 $L \cdot mol^{-1} \cdot h^{-1}$). In fact, it is hard to understand why the duplex spacer led to a slower hybridization in the case of system 3. A simplified scenario might be that the reduced overall flexibility and confined spatial movement of the double-stranded DNA ligands decreased their ability to find a correctly oriented DNA complement. Another possibility was attributed to the Mfold-predicted existence of a relatively stable hairpin conformation for the ss-3 strand[57], with a melting temperature slightly above 4 ℃ (see Electronic Supplementary Material). The formation of a duplex spacer might stabilize such a folding by base-stacking (but disfavored by some unpaired free bases at the stacking site, see Electronic Supplementary Material for details) such that the hybridization between ss-3 and ss-3c was somehow suppressed. In the case of system 4,

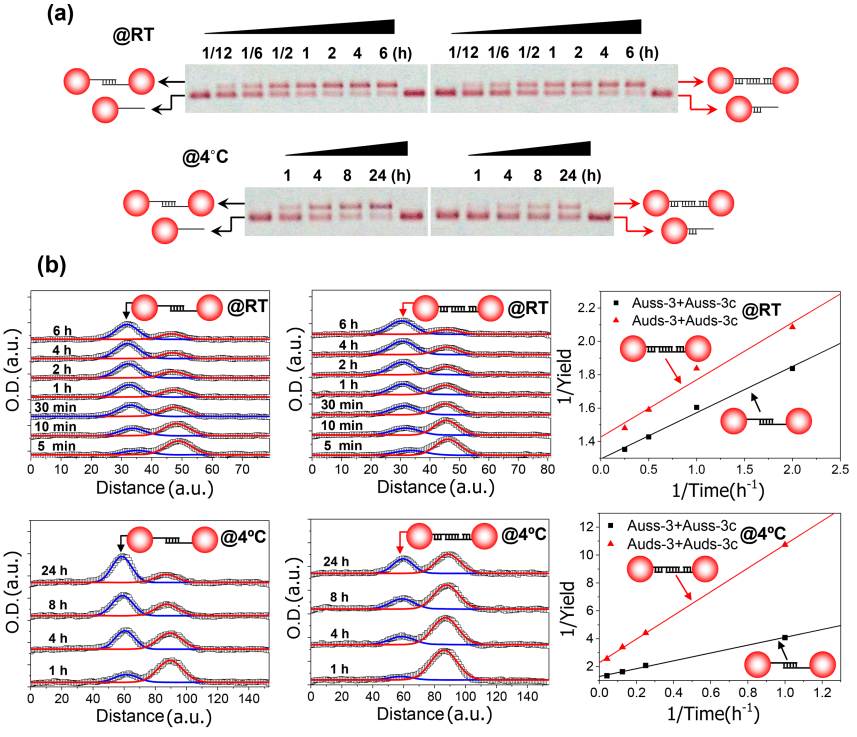

Figure 3. Gel electrophoretic analysis of the hybridization kinetics for system 3. (a) 3% agarose gel electrophoretic separations of the dimerization products of 5 nm gold nanoparticles corresponding to different reaction durations. Each nanoparticle bears a single DNA ligand with an either single or double stranded DNA spacer domain proximal to the gold surface. (b) Digitized gel electropherograms and corresponding kinetic plots to extract kinetic constants. DNA sequences for system 3: ss-3: CACGCATAGGTCCTG-T_{15}-SH (5'-3'); ss-3c: CAGGACCTATGCGTG-T_{15}-SH (5'-3'). The double stranded spacer is formed by hybridizing ss-3 and ss-3c with an A_{15} complement. Auss and Auds represent DNA-monoconjugated AuNPs with single and doubled stranded spacer domains, respectively.

the effect of the double or single stranded DNA spacer on the hybridization kinetics followed a normal order. However, this system gave the smallest kinetic constants. At room temperature (18 ℃), the k_{app}^{ss} (9.92×10^{6} L · mol^{-1} · h^{-1}) and k_{app}^{ds} (1.51×10^{7} L · mol^{-1} · h^{-1}) of system 4 were about 10-time smaller than system 1. This difference was further boosted by another order when the assembly was carried out at 4 ℃ such that an overall 100-time kinetic variation was resulted among the four systems. We did not find any stable secondary conformations for system 4 that might cause such a huge kinetic difference based on the Mfold program (see Electronic Supplementary Material)[57]. In addition, the melting points of these systems were also similar (Figure S13). Surface adsorption and base stacking should not be the reason as the difference between k_{app}^{ss} and k_{app}^{ds} was even smaller for system 4, in comparison with systems 1 and 2. This unexplainable phenomenon might be related to the cooperative actions of multiple factors including some "hidden" ones to be revealed in the future.

To decipher the role of base stacking in the promoted hybridization kinetics, we modified system 1 by adding an extra base between the hybridization and spacer sequences for each of the two strands. Such an alteration led to two 31-base long DNA sequences named as ss-5 and ss-5c in system 5 (Figure 5). A hybridized structure between these two strands with duplex (T_{15}/A_{15}) spacers contains two unpaired G and C bases interfacing the hybridization and spacer domains. Consequently, base stacking could be suppressed at these two sites each having a redundant base. By carrying out the AGE-based dimerization assay for system 5, hybridization kinetic constants were obtained. The apparent rate constants of k_{app}^{ss} and k_{app}^{ds} were found to be 1.39×10^{8} and 2.06×10^{8} L · mol^{-1} · h^{-1}, at room temperature, respectively. Accordingly, a kinetic enhancement factor of 1.48 was obtained for the DNA-AuNP conjugates with double-stranded spacers in comparison with single-stranded ones. Keeping in mind that a 2.21-time enhancement was observed for system 1, the kinetic promotion of 1.48 for system 5 in the absence of base stacking became less significant. These data clearly revealed an important role of base stacking in the hybridization of DNA-AuNP complexes, which accounted roughly for one-half ((2.21−1.48)/(2.21−

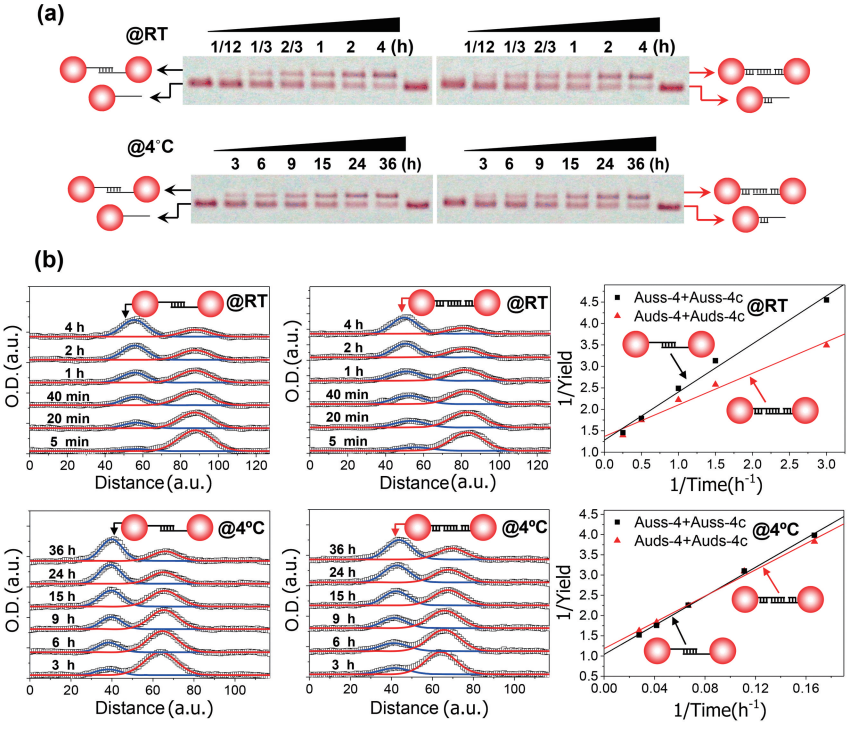

Figure 4. Gel electrophoretic analysis of the hybridization kinetics for system 4. (a) 3% agarose gel electrophoretic separations of the dimerization products of 5 nm gold nanoparticles corresponding to different reaction durations. Each nanoparticle bears a single DNA ligand with an either single or double stranded DNA spacer domain proximal to the gold surface. (b) Digitized gel electropherograms and corresponding kinetic plots to extract kinetic constants. DNA sequences for system 4: ss-4: TATCGCTGACTCTAC-T_{15}-SH (5'-3'); ss-4c: GTAGAGTCAGCGATA-T_{15}-SH (5'-3'). The double stranded spacer is formed by hybridizing ss-4 and ss-4c with an A_{15} complement. Auss and Auds represent DNA-monoconjugated AuNPs with single and doubled stranded spacer domains, respectively.

1) = 60%) of the observed kinetic enhancement for system 1. The remaining half of the kinetic promotion could then be attributed to a suppressed interaction (e.g. adsorption) between DNA and gold surface. Similarly, lowering the reaction temperature for system 5 led to decreased k_{app}^{ss} (7.47×10^{7} L · mol^{-1} · h^{-1}) and k_{app}^{ds} (1.01×10^{8} L · mol^{-1} · h^{-1}), in consistent with systems 1 – 4. At such a lowered temperature, an enhancement factor of 1.35 by using double-stranded spacers was achieved.

The above analyses assumed that all DNA-AuNP monomers are reactive, and able to hybridize into dimers given long enough waiting time. However, due to yet unidentified reasons (possibly relevant to the existence of DNA-free AuNPs or surface-anchored DNA bases), there is always a certain amount of unreactive reactants in the dimerization reaction (Eq. (1)). This situation caused the intercept on the $1/Y$ axis of the linear plot in Eq. (3) to be deviated from "1". If we assume identical percentages (denoted as "c") of the unreacted nanospecies in a complementary pair of DNA-AuNP monomers, a corrected form of Eq. (3) is easily derived:

$$\frac{1}{Y}=\frac{[A]_0}{[P]}=\frac{1}{k_{app}[A]_0(1-c)^2}\cdot\frac{1}{t}+\frac{1}{1-c} \quad (5)$$

Accordingly, the ratio "c" representing unreactive AuNPs in a dimerization process can be inferred from the intercept "$1/(1-c)$" of the $1/Y \sim 1/t$ linear fitting based on Eq. (5), which is then combined with the slope to obtain k_{app}. The corrected values of k_{app} for systems 1-5 were listed in Table 1. While the general trends of duplex-spacer-enhanced kinetics and their strong sequence-dependency were still very clear, some differences could be noticed. In the case of system 5, the kinetic difference between single and double stranded spacers almost disappeared, which further ascertained the important role of base stacking in promoting hybridization kinetics. In the meantime, the reversed kinetic order of system 3 for the single- and double-stranded spacers now became normal. Such a result tended to support the rationality of Eq. (5), though the assumption of identical "c" for two reactants in a dimerization reaction is somehow tentative (but seems to be a good approximation).

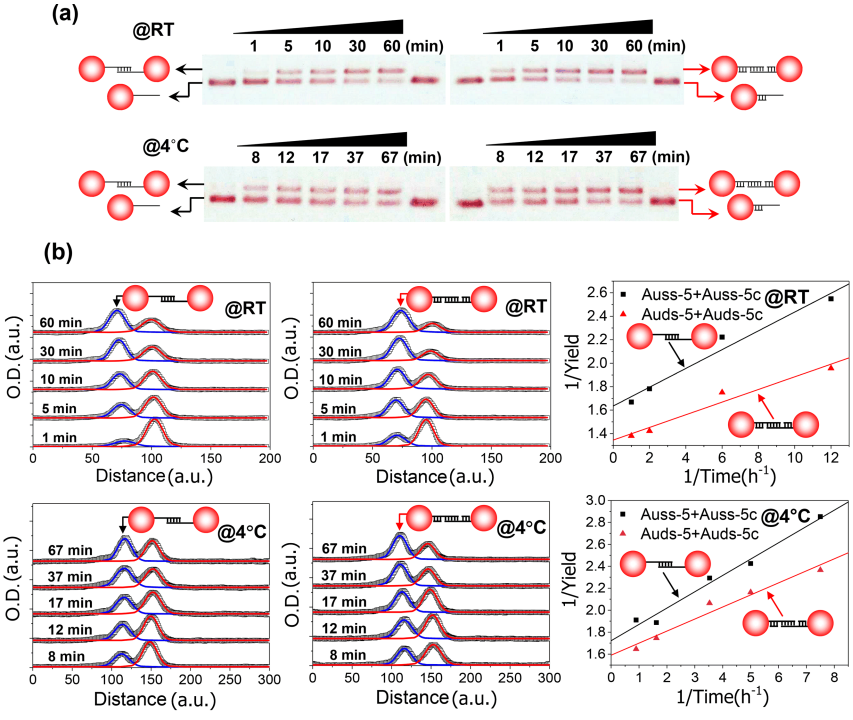

Figure 5. Gel electrophoretic analysis of the hybridization kinetics for system 5. (a) 3% agarose gel electrophoretic separations of the dimerization products of 5 nm gold nanoparticles corresponding to different reaction durations. Each nanoparticle bears a single DNA ligand with an either single or double stranded DNA spacer domain proximal to the gold surface. (b) Digitized gel electropherograms and corresponding kinetic plots to extract kinetic constants. DNA sequences for system 5: ss-5: TACTTCCAATCCAATC-T_{15}-SH (5'-3'); ss-5c: ATTGGATTGGAAGTAG-T_{15}-SH (5'-3'). The double stranded spacer is formed by hybridizing ss-5 and ss-5c with an A_{15} complement. Auss and Auds represent DNA-monoconjugated AuNPs with single and doubled stranded spacer domains, respectively.

Table 1. The measured kinetic constants for systems 1-5 with single and doubled stranded DNA spacers at two reaction temperatures of RT (room temperature) and 4 ℃.

Temperature	Spacer	k_{app}(L·mol^{-1}·h^{-1}) (system1)	k_{app}(L·mol^{-1}·h^{-1}) (system2)	k_{app}(L·mol^{-1}·h^{-1}) (system 3)	k_{app}(L·mol^{-1}·h^{-1}) (system4)	k_{app}(L·mol^{-1}·h^{-1}) (system5)
RT	T_{15}	7.55×10^{7}	2.62×10^{7}	4.01×10^{7}	9.92×10^{6}	1.39×10^{8}
		$(1.15\times10^{8})^{a}$	$(3.32\times10^{7})^{a}$	$(6.72\times10^{7})^{a}$	$(1.63\times10^{7})^{a}$	$(3.71\times10^{8})^{a}$
	T_{15}/A_{15}	1.67×10^{8}	6.52×10^{7}	3.24×10^{7}	1.51×10^{7}	2.06×10^{8}
		$(2.27\times10^{8})^{a}$	$(9.78\times10^{7})^{a}$	$(6.58\times10^{7})^{a}$	$(2.83\times10^{7})^{a}$	$(3.73\times10^{8})^{a}$
4 ℃	T_{15}	4.01×10^{7}	1.01×10^{7}	3.95×10^{6}	6.20×10^{5}	7.47×10^{7}
		$(5.82\times10^{7})^{a}$	$(1.64\times10^{7})^{a}$	$(6.53\times10^{6})^{a}$	$(6.70\times10^{5})^{a}$	$(2.21\times10^{8})^{a}$
	T_{15}/A_{15}	5.06×10^{7}	1.39×10^{7}	1.31×10^{6}	6.85×10^{5}	1.01×10^{8}
		$(6.55\times10^{7})^{a}$	$(2.51\times10^{7})^{a}$	$(6.81\times10^{6})^{a}$	$(9.59\times10^{5})^{a}$	$(2.56\times10^{8})^{a}$

[Note] [a] Corrected for non-unit intercepts according to Eq. (5).

4 Conclusions

The kinetic constants (Table 1, Figure 6) and the $k_{app}^{ds}/k_{app}^{ss}$ ratios (Figure 6) were compared among five systems, based on which the following conclusions can be drawn. (i) Similar to DNA-multifunctionalized systems, a double stranded spacer proximal to gold surface is generally effective in promoting the hybridizability of the terminal DNA sequences on monovalent DNA-AuNP conjugates. Both suppressed ligand adsorption and the base stacking between the spacing and hybridizing domains can contribute to such an improvement. However, this rule may not always be true, and can be reversed in certain cases (e.g. system

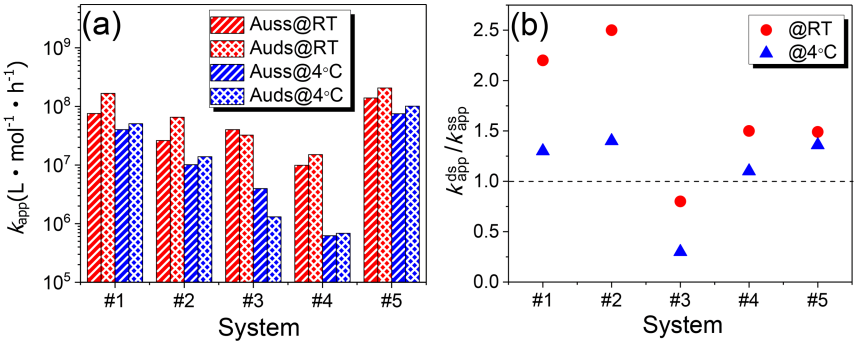

Figure 6. (a) Comparisons of kinetic constants (k_{app}) for systems 1 to 5 at different temperatures. (b) The ratios of as-measured kinetic constants ($k^{ds}_{app}/k^{ss}_{app}$) for DNA ligands with double and single stranded spacer domains.

3). (ii) The hybridization sequence has an even more dramatic influence on the dimerization kinetics, which can cause a big variation of rate constants up to two orders. Therefore, it is the base sequence (not the spacer rigidity) that plays a more important role in determining the hybridizability of DNA-monoconjugated AuNPs. Note that the sequence-dependency observed in our systems has excluded the influence of secondary DNA conformations. (iii) A decreased hybridization temperature slows down a hybridization reaction, and the difference between double and single stranded DNA spacers diminishes at a lowered temperature. This result is better explained by the base stacking effect rather than the suppressed adsorption. In an exceptional case (e.g. system 3), the difference between single and double stranded spacers is even enhanced at a lowered temperature but with a reversed kinetic order. These findings point out that the surface adsorption of DNA bases, the base stacking at a nick site of the DNA linkage, the inherent hybridizability of specific DNA sequences, and the confined spatial movement of the DNA ligands all could contribute to the assembly kinetics of DNA-monoconjugated NPs. (iv) By taking into consideration of possibly existing unreactive AuNP species in a dimerization reaction, the role of kinetic promotion by the base stacking effects at the two interfaces of hybridization and spacer domains is further highlighted. Our work reveals a great complexity of hybridization kinetics even for the simplest (monovalent) DNA-AuNP conjugates, which has not been studied before. While some mechanistic understandings are still quite plausible, the dimerization-based kinetic assay will enable a rapid, reliable, and high-throughput pre-screening of candidate DNA sequences for analytical, biological, and nanotechnological applications. Also, the seemingly unexplainable sequence dependency of hybridization kinetics might be predictable based on artificial intelligence techniques such as machine learning. With a further development of theoretical tools[41,58,59] and a more quantitative understanding (or complete removal) of unreactive DNA-nanoparticle conjugates from the reaction systems, we believe the kinetic complexity revealed by the present work may be gradually clarified.

Supplementary data

Supplementary data are available at J. Univ. Sci. Tech. China online.

Acknowledgments

This work was supported by the National Key Research and Development Program of China (2021YFA1200101, 2018YFA0702001) and the National Natural Science Foundation of China (21972130, 21521001, 21425521).

Conflict of interest

The authors declare no conflict of interest.

Author information

WANG Jiannan and ZHENG Yuanqin are co-first authors.

WANG Jiannan is a master student under the supervision of Prof. DENG Zhaoxiang at University of Science and Technology of China. Her research mainly focuses on nanosynthesis and DNA-directed nanoassembly.

ZHENG Yuanqin received her PhD from University of Science and Technology of China in 2012. She is currently working at Hefei University of Technology.

DENG Zhaoxiang (corresponding author) received his PhD from University of Science and Technology of China in 2000. He is currently a professor at University of Science and Technology of China. His research focuses on DNA nanotechnology and its analytical applications.

References

[1] Jones M R, Seeman N C, Mirkin C A. Programmable materials and the nature of the DNA bond. Science, 2015, 347(6224): 1260901.

[2] Zhang F, Nangreave J, Liu Y, et al. Structural DNA nanotechnology: state of the art and future perspective. J. Am. Chem. Soc., 2014, 136(32): 11198-11211.

[3] Seeman N C. Structural DNA Nanotechnology. Cambridge: Cambridge University Press, 2016.

[4] Lin Q Y, Mason J A, Li Z Y, et al. Building superlattices from individual nanoparticles via template-confined DNA-mediated assembly. Science, 2018, 359(6376): 669-672.

[5] Young K L, Ross M B, Blaber M G, et al. Using DNA to design plasmonic metamaterials with tunable optical properties. Adv. Mater., 2014, 26(4): 653-659.

[6] Fan J A, Wu C, Bao K, et al. Self-assembled plasmonic

nanoparticle clusters. Science, 2010, 328(5982): 1135-1138.
[7] Lu C H, Willner B, Willner I. DNA nanotechnology: From sensing and DNA machines to drug-delivery systems. ACS Nano, 2013, 7(10): 8320-8332.
[8] Keyser U F. Enhancing nanopore sensing with DNA nanotechnology. Nat. Nanotech., 2016, 11(2): 106-108.
[9] Pilo-Pais M, Acuna G P, Tinnefeld P, et al. Sculpting light by arranging optical components with DNA nanostructures. MRS Bull., 2017, 42: 936-942.
[10] Zhou C, Duan X Y, Liu N. DNA-nanotechnology-enabled chiral plasmonics: From static to dynamic. Acc. Chem. Res., 2017, 50(12): 2906-2914.
[11] Han X G, Zhou Z H, Yang F, et al. Catch and release: DNA tweezers that can capture, hold and release an object under control. J. Am. Chem. Soc., 2008, 130: 14414-14415.
[12] Zhang C, Macfarlane R J, Young K L, et al. A general approach to DNA-programmable atom equivalents. Nat. Mater., 2013, 12(8): 741-746.
[13] Zhang Y, Lu F, Yager K G, et al. A general strategy for the DNA-mediated self-assembly of functional nanoparticles into heterogeneous systems. Nat. Nanotechnol., 2013, 8(11): 865-872.
[14] Chen G L, Wang S, Song L, et al. Pt supraparticles with controllable DNA valences for programmed nanoassembly. Chem. Commun., 2017, 53(70): 9773-9776.
[15] Zheng Y Q, Li Y L, Deng Z X. Silver nanoparticle-DNA bionanoconjugates bearing a discrete number of DNA ligands. Chem. Commun., 2012, 48(49): 6160-6162.
[16] Li Y L, Zheng Y Q, Gong M, et al. Pt nanoparticles decorated with a discrete number of DNA molecules for programmable assembly of Au-Pt bimetallic superstructures. Chem. Commun., 2012, 48(31): 3727-3729.
[17] Wang H Q, Li Y L, Gong M, et al. Core solution: A strategy towards gold core/non-gold shell nanoparticles bearing strict DNA-valences for programmable nanoassembly. Chem. Sci., 2014, 5(3): 1015-1020.
[18] Wang H Q, Deng Z X. Gel electrophoresis as a nanoseparation tool serving DNA nanotechnology. Chin. Chem. Lett., 2015, 26(12): 1435-1438.
[19] Tikhomirov G, Hoogland S, Lee P E, et al. DNA-based programming of quantum dot valency, self-assembly and luminescence. Nat. Nanotechnol., 2011, 6(8): 485-490.
[20] Pal S, Sharma J, Yan H, et al. Stable silver nanoparticle-DNA conjugates for directed self-assembly of core-satellite silver-gold nanoclusters. Chem. Commun., 2009(40): 6059-6061.
[21] Zhang X, Servos M R, Liu J. Fast pH-assisted functionalization of silver nanoparticles with monothiolated DNA. Chem. Commun., 2012, 48(81): 10114-10116.
[22] Deng Z, Pal S, Samanta A, et al. DNA functionalization of colloidal II-VI semiconductor nanowires for multiplex nanoheterostructures. Chem. Sci., 2013, 4(5): 2234-2240.
[23] Li L, Wu P, Hwang K, et al. An exceptionally simple strategy for DNA-functionalized up-conversion nanoparticles as biocompatible agents for nanoassembly, DNA delivery, and imaging. J. Am. Chem. Soc., 2013, 135(7): 2411-2414.
[24] Song L, Deng Z X. Valency control and functional synergy in DNA-bonded nanomolecules. ChemNanoMat, 2017, 3(10): 698-712.
[25] Hao Y, Li Y J, Song L, et al. Flash synthesis of spherical nucleic acids with record DNA density. J. Am. Chem. Soc., 2021, 143(8): 3065-3069.
[26] Liao Y H, Lin C H, Cheng C Y, et al. Monovalent and oriented labeling of gold nanoprobes for the high-resolution tracking of a single-membrane molecule. ACSNano, 2019, 13(10): 10918-10928.
[27] Howarth M, Liu W H, Puthenveetil S, et al. Monovalent, reduced-size quantum dots for imaging receptors on living cells. Nat. Methods, 2008, 5(5): 397-399.
[28] Takashimaa A, Oishi M. Kinetic study of DNA hybridization on DNA-modified gold nanoparticles with engineered nano-interfaces. RSC Adv., 2015, 5(93): 76014-76018.
[29] Leunissen M E, Dreyfus R, Sha R, et al. Quantitative study of the association thermodynamics and kinetics of DNA-coated particles for different functionalization schemes. J. Am. Chem. Soc., 2010, 132(6): 1903-1913.
[30] Chen C, Wang W, Ge J, et al. Kinetics and thermodynamics of DNA hybridization on gold nanoparticles. Nucleic Acids Res., 2009, 37(11): 3756-3765.
[31] Elghanian R, Storhoff J J, Mucic R C, et al. Selective colorimetric detection of polynucleotides based on the distance-dependent optical properties of gold nanoparticles. Science, 1997, 277(5329): 1078-1081.
[32] Park S, Brown K A, Hamad-Schifferli K. Changes in oligonucleotide conformation on nanoparticle surfaces by modification with mercaptohexanol. Nano Lett., 2004, 4(10): 1925-1929.
[33] Liu B W, Wu P, Huang Z C, et al. Bromide as arobust backfiller on gold for precise control of DNA conformation and high stability of spherical nucleic acids. J. Am. Chem. Soc., 2018, 140(13): 4499-4502.
[34] Maye M M, Nykypanchuk D, van der Lelie D, et al. A simple method for kinetic control of DNA-induced nanoparticle assembly. J. Am. Chem. Soc., 2006, 128(43): 14020-14021.
[35] Prigodich A E, Lee O S, Daniel W L, et al. Tailoring DNA structure to increase target hybridization kinetics on surfaces. J. Am. Chem. Soc., 2010, 132(31): 10638-10641.
[36] Li Y L, Han X G, Deng Z X. Grafting SWNTs with highly hybridizable DNA sequences: Potential building blocks for DNA-programmed material assembly. Angew. Chem. Int. Ed., 2007, 46(39): 7481-7484.
[37] Maune H T, Han S P, Barish R D, et al. Self-assembly of carbon nanotubes into two-dimensional geometries using DNA origami templates. Nat. Nanotech., 2010, 5(1): 61-66.
[38] Sun W, Shen J, Zhao Z, et al. Precise pitch-scaling of carbon nanotube arrays within three-dimensional DNA nanotrenches. Science, 2020, 368(6493): 874-877.
[39] Zhang J X, Fang J X, Duan W, et al. Predicting DNA hybridization kinetics from sequence. Nat. Chem., 2018, 10(11): 91-98.
[40] Esashika K, Saiki T. DNA Hybridization assay using gold nanoparticles and electrophoresis separation provides 1 pM sensitivity. Bioconjug. Chem., 2018, 29(1): 182-189.
[41] Marimuthu K, Chakrabarti R. Sequence-dependent theory of oligonucleotide hybridization kinetics. J. Chem. Phys., 2014, 140(17): 175104.
[42] Sorgenfrei S, Chiu C Y, Gonzalez Jr R L, et al. Label-free field-effect-based single-molecule detection of DNA hybridization kinetics. Nat. Nanotechnol., 2011, 6(2): 126-132.
[43] Yin Y D, Zhao X S. Kinetics and dynamics of DNA hybridization. Acc. Chem. Res., 2011, 44(1): 1172-

1181.
[44] Lee C Y, Nguyen P C, Grainger D W, et al. Structure and DNA hybridization properties of mixed nucleic acid/maleimide-ethylene glycol monolayers. Anal. Chem., 2007, 79(12): 4390-4400.
[45] Erickson D, Li D Q, Krull U J. Modeling of DNA hybridization kinetics for spatially resolved biochips. Anal. Biochem., 2003, 317(2):186-200.
[46] Okahata Y, Kawase M, Niikura K, et al. Kinetic measurements of DNA hybridization on an oligonucleotide-immobilized 27-MHz quartz crystal microbalance. Anal. Chem., 1998, 70(7): 1288-1296.
[47] Schwille P, Oehlenschläger F, Walter N G. Quantitative hybridization kinetics of DNA probes to RNA in solution followed by diffusional fluorescence correlation analysis. Biochemistry, 1996, 35(31): 10182-10193.
[48] Mazumder A, Majlessi M, Becker M M. A high throughput method to investigate oligodeoxyribonucleotide hybridization kinetics and thermodynamics. Nucleic Acids Res., 1998, 26(8): 1996-2000.
[49] Yao G B, Li J, Li Q, et al. Programming nanoparticle valence bonds with single-stranded DNA encoders. Nat. Mater., 2020, 19(7): 781-788.
[50] Zanchet D, Micheel C M, Parak W J, et al. Electrophoretic isolation of discrete Au nanocrystal/DNA conjugates. Nano Lett., 2001, 1(1): 32-35.
[51] Claridge S A, Liang H W, Basu S R, et al. Isolation of discrete nanoparticle-DNA conjugates for plasmonic applications. Nano Lett., 2008, 8(4): 1202-1206.
[52] Kushon S A, Jordan J P, Seifert J L, et al. Effect of secondary structure on the thermodynamics and kinetics of PNA hybridization to DNA hairpins. J. Am. Chem. Soc., 2001, 123(44): 10805-10813.
[53] Riccelli P V, Merante F, Leung K T, et al. Hybridization of single-stranded DNA targets to immobilized complementary DNA probes: comparison of hairpin versus linear capture probes. Nucleic Acids Res., 2001, 29(4): 996-1004.
[54] Gao Y, Wolf L K, Georgiadis R M. Secondary structure effects on DNA hybridization kinetics: A solution versus surface comparison. Nucleic Acids Res., 2006, 34(11): 3370-3377.
[55] Alivisatos A P, Johnsson K P, Peng X G, et al. Organization of ´nanocrystal molecules´ using DNA. Nature, 1996, 382: 609-611.
[56] Yuan B F, Zhuang X Y, Hao Y H, et al. Kinetics of base stacking-aided DNA hybridization. Chem. Commun., 2008, (48): 6600-6602.
[57] Zuker M. Mfold web server for nucleic acid folding and hybridization prediction. Nucleic Acids Res., 2003, 31(13): 3406-3415.
[58] Markegard C B, Gallivan C P, Cheng D D, et al. Effects of concentration and temperature on DNA hybridization by two closely related sequences via large-scale coarse-grained simulations. J. Phys. Chem. B, 2016, 120(32): 7795-7806.
[59] Markegard C B, Fu I W, Reddy K A, et al. Coarse-grained simulation study of sequence effects on DNA hybridization in a concentrated environment. J. Phys. Chem. B, 2015, 119(5): 1823-1834.

单价 DNA 偶联纳米粒子序列依赖的杂交活性：二聚组装揭示动力学复杂性

王建楠，郑园琴，李育林，邓兆祥*
中国科学技术大学化学系，生物分析化学中心，安徽合肥 230026
* 通讯作者. E-mail：zhxdeng@ustc.edu.cn

摘要：理解 DNA 杂交动力学对诸多研究具有重要意义，例如核酸检测、基因生物技术和 DNA 纳米技术等. DNA 偶联纳米材料丰富了可编程纳米组装结构的功能性，且可实现生物分析和纳米技术应用的超精细控制. 尽管末端标记小分子不会对 DNA 的杂交能力造成太大影响，但与纳米粒子偶联会显著抑制 DNA 链杂交动力学. DNA 杂交受阻不仅降低了复杂纳米结构的构建效率，还会使传感器和纳米马达等响应缓慢. 以 DNA 单价偶联纳米粒子作为理想体系，本文尝试使用琼脂糖凝胶电泳分析研究 DNA 杂交驱动二聚组装过程的动力学复杂性，揭示了影响 DNA 杂交反应的多个共存因素. 这些因素包括：靠近纳米粒子表面 DNA 间隔区的刚性；DNA 间隔区和杂交区之间发生碱基堆积；固有的碱基序列依赖的杂交活性；DNA 杂交序列空间运动的受限性. 本研究为 DNA 功能化纳米材料提供了一种可靠的杂交动力学评价策略，可望为发展结构复杂且响应快速的功能分析器件和高性能生物标记纳米探针提供重要保障.

关键词：电泳；DNA；杂交动力学；纳米粒子；单价偶联